

# Geomagnetic activity during St. Patrick's Day storm inferred from global and local indicators

A. D. Gvishiani<sup>1</sup>, R. V. Sidorov<sup>1</sup>, R. Yu. Lukianova<sup>1</sup>, and A. A. Soloviev<sup>1</sup>

Received 16 December 2016; accepted 19 December 2016; published 23 December 2016.

In this research, the comparison between the results of geomagnetic activity monitoring using the new local indicators of geomagnetic activity and the traditional geomagnetic indices for geomagnetic activity analysis is made for the period of the strongest geomagnetic disturbance of the current solar cycle – the St. Patrick's Day storm (17–18 March 2015). The results of the research demonstrated that the classification of magnetic activity using the mentioned indicators does not contradict the classical methods. The local indicators, applied to recognition of disturbances in the magnetic observatory data, seem an effective tool for geomagnetic activity analysis, as they reveal the characteristic features of geomagnetic disturbances typical for the observatory latitudinal location and show agreement the conventional geomagnetic disturbance distribution and its evolution during a magnetic storm. **KEYWORDS:** Geomagnetic storm; geomagnetic activity; local geomagnetic activity indicators; discrete mathematical analysis.

**Citation:** Gvishiani, A. D., R. V. Sidorov, R. Yu. Lukianova, and A. A. Soloviev (2016), Geomagnetic activity during St. Patrick's Day storm inferred from global and local indicators, *Russ. J. Earth. Sci.*, 16, ES6007, doi:10.2205/2016ES000593.

## 1. Introduction

Geomagnetic storms are major space weather events. Storms are well known to be more frequent during the solar maximum and declining phase of the 11-yr solar cycle (SC). Strong storms are associated with the passage of fast coronal mass ejections (CMEs) [Richardson and Cane, 2012]. The ejected magnetic cloud (MC) carries strong southward interplanetary magnetic field (IMF) which drives enhanced reconnection with the Earth's magnetic field and supplies a great amount of energy the Earth's magnetosphere [Dungey, 1961]. It results in intense geomagnetic activity including substorm-associated electric current wedge and ring current build-up.

During the last solar minimum, 2007–2009, the sunspot number (SSN) was extremely low and no major geomagnetic storm was recorded. Then, the next SC, SC 24, started. The SSN gradually increased and reached a maximum of SC 24 in 2012. During the declining phase of SC 24, on March 17, 2015, which happens to be St. Patrick's Day, the strongest

geomagnetic storm of SC 24 occurred following a CME impact. The storm was rated G4 (“severe”) on the five-level NOAA space weather scale, geomagnetic disturbances were considerably strong throughout the world, and very active aurora were reported from surprisingly low latitudes. The St. Patrick's Day storm represents a good case study to investigate the changes in the features of the magnetic field fluctuations recorded by the magnetometers.

In this study we analyze the geomagnetic effect of the St. Patrick's Day storm using the traditional geomagnetic indices and the local indicators of geomagnetic activity calculated from the data of Russian observatories. Only the observatories of the INTERMAGNET standard are considered. At present twelve Russian observatories are able to provide the high world-quality measurements of the Earth's magnetic field which satisfy the requirements of INTERMAGNET [Rasson, 2001]. The data are collected using a new geomagnetic Hardware and Software System (HSS) which was developed in 2014–2016 for the efficient and automated retrieval, storage, processing, and analysis for geomagnetic data [Gvishiani *et al.*, 2014, 2016b]. It provides the online access to geomagnetic data (both, the initial and processed ones), a sophisticated classification of the extreme geomagnetic events, detection of extreme geomagnetic conditions and visualization of the results.

<sup>1</sup>Geophysical Center RAS, Moscow, Russia

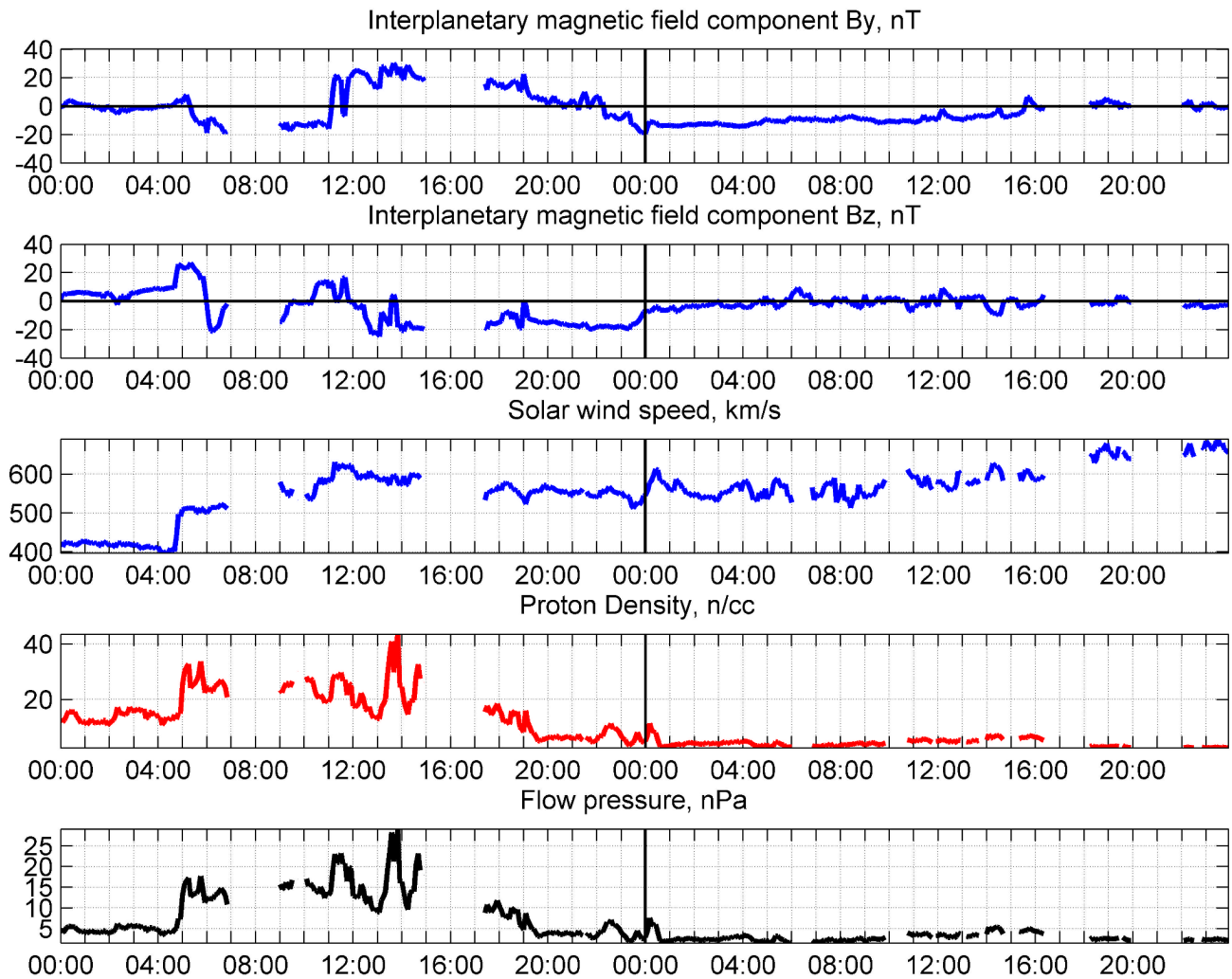


**Figure 1.** Solar wind 5-min parameters from OMNI database for 17–18 March, 2015. The horizontal axis labels are the UT hours within the daily periods.

## 2. Space Weather Conditions During the St. Patrick's Day Geomagnetic Storm

### 2.1 Interplanetary Conditions

To describe the space weather conditions during the storm, in Figure 1 we plot the IMF  $B_z$  and  $B_y$  components, the solar wind speed, density and dynamic pressure on March 17–18, 2015. The solar wind data were downloaded from the OMNIWeb website (<http://omniweb.gsfc.nasa.gov/>) of the NASA Goddard Space Flight Center. The magnetic field and plasma data are 5-min-averaged, shifted to the Earth's magnetopause nose. Two gaps at 0700–0900 UT and 1500–1700 UT, March 17 are likely caused by a saturation of the particle analyzer due to extreme solar wind.

It is well known that the southward component of the IMF plays a major role in the generation of geomagnetic storms.

On March 17 the initially conditions did not look favorable, however the IMF  $B_z$  component soon began to point sharply south for long periods which persisted for many hours during the main phase of the geomagnetic storm. The arrival of interplanetary shock at the nose of Earth magnetosphere produced a storm sudden commencement (SSC) at 0445 UT. At the same time the solar wind speed as measured by ACE spacecraft increased to above 500 km/s, while the IMF  $B_z$  was initially pointing north ( $B_z = +25$  nT at 0500 UT, March 17), a condition known to suppress geomagnetic activity. An abrupt increase of the solar wind speed matches the proton density front and the corresponding flow pressure increases. The pressure was enhanced until the end of March 17 with a maximum of 30 nPa occurred at 1330 UT. The solar wind speed gradually increased up to 600 km/s on March 17 and then up to 700 km/s.

The storm started at 0600 UT right after the IMF turned southward. At 0615 UT  $B_z$  reached the local minimum of  $-20$  nT. Later, shortly after the IMF turned northward, the

storm slightly recovered. Then, at 1220 UT the IMF turned southward again and caused the second storm intensification. Thus this event was a two-step storm. The first step was associated with a southward IMF embedded in the MC front region, whereas the second, more prolonged step was associated with a southward IMF within MC. The IMF  $B_z$  was continuously negative (about  $-20$  nT) until the end of March 17 and close to zero on March 18. During the first storm intensification, at 0500–1100 UT, the IMF azimuthal ( $B_y$ ) component was strongly negative (below  $-20$  nT). At 1100 UT it abruptly turned to the opposite direction and reached  $+20$  nT. In the end of March 17 the IMF  $B_y$  again became negative and after that stayed continuously negative for many hours.

Evolution of solar wind parameters presented in Figure 1 indicates that the storm was driven by a large amount of energy penetrating the magnetosphere due to intense magnetic reconnection during a prolonged period of strongly southward IMF accompanied and followed by high speed streams.

## 2.2 Global Geomagnetic Activity

Energetic interaction between the solar wind and the Earth's magnetosphere causes a movement of plasma through the magnetosphere and generation of electric currents which drive a strong geomagnetic activity. To estimate the global geomagnetic activity we use four basic geomagnetic indices: the  $K_p$  [Menvielle and Berthelier, 1991],  $AE$  [Davis and Sugiura, 1966],  $SYM/H$  [Iyemori, 1992] and  $PC$  [Troshichev et al., 1988] indices. Each index describes the magnetic activity at different latitudes caused by a particular current system in the ionosphere and magnetosphere.

The planetary three-hour-range  $K_p$  index was introduced by J. Bartels in 1950s and is derived from the standardized  $K$  index of 13 midlatitude magnetic observatories in Northern and Southern hemispheres. The planetary  $K_p$  index is designed to measure magnetic effects of the ionospheric currents mostly caused by solar particle radiation and provides an objective estimation of geomagnetic activity in a quasi-logarithmic scale. The  $AE$  (Auroral Electrojet) index was originally introduced as a measure of global electrojet activity in the auroral zone. The  $AE$  index is derived from geomagnetic variations in the horizontal component observed at selected (10–13) observatories along the auroral zone in the northern hemisphere. The  $PC$  (Polar Cap) index is a characteristic of the polar cap magnetic activity generated by geoeffective solar wind acting on the magnetosphere. The index is derived by magnetic data of only two stations Thule and Vostok located in the northern and southern near-pole regions. The  $SYM/H$  index is the 1-min analog of the 1-hr  $Dst$  index which represents the magnetic effect of the storm-time magnetospheric ring current. The index is derived for  $H$  magnetic component measured at four low latitude observatories.

Figure 2 depicts the high latitude  $PC$  and  $AE$  indices, the low latitude  $SYM/H$  index and the planetary midlatitude  $K_p$  index for the period of March 17–18, 2015. During the storm all indices are disturbed. A relatively good agreement is between the variation of  $PC$  and  $AE$  indices. There

are several enhancements in both indices that are associated with strong intensifications of the substorms occurred in the course of the main and recovery phases of the storm. The largest peak in  $PC$  (up to 15 mV/m) and  $AE$  (up to 2000 nT) occurred at 1400 UT on March 17. The  $SYM/H$  sharply increases at 0445 UT indicating a beginning of an unusually prolonged SSC. Because at the front of MC the IMF was strongly northward the storm started almost 2 hours later. At 0900 UT the  $SYM/H$  reached its first minimum of  $-100$  nT. After that the index slightly increased and then again decreased below  $-220$  nT at 2300 UT. Thus during the St. Patrick's Day storm there were two intensifications of the ring current and the storm was actually the two-step one. The  $K_p$  index indicates the enhanced magnetic activity ( $K_p > 4$ ) over the globe starting from the SSC and persisting till the end of March 18. The largest  $K_p$  (up to 8–) are characteristic of the second step of the storm main phase at 1400–2400 UT. During this period there were four substorm intensifications when the  $AE$  increased up to 1500 nT.

All four geomagnetic indices indicate the development of intense two-step geomagnetic storm accompanied by several intense auroral and polar substorms. All latitudes were affected.

## 2.3 Geomagnetic Activity by the Local Indicators

An individual observatory measures the orthogonal geomagnetic components and the total intensity of the geomagnetic field. These data can be transformed into the local indicators of geomagnetic activity. The new indicators are calculated using the mathematical approaches of the discrete mathematical analysis (DMA). The DMA is based on the fuzzy logic and includes a series of algorithms aimed at basic tasks of data analysis. The DMA algorithms enable a morphological analysis of the time series, a detection of the formal anomalies and an estimation of the trends [Bogoutdinov et al., 2010; Soloviev et al., 2009, 2012a, 2012b, 2013; Zelinskiy et al., 2014]. The DMA has been previously used for the geophysical monitoring [Agayan et al., 2016; Gvishiani et al., 2014, 2016a, 2016b; Soloviev et al., Estimation of geomagnetic activity..., Annals of Geophysics, in press], for the data processing [Agayan et al., 2010, 2014; Gvishiani et al., 2011], and for solution of various other problems which arise in the practice of geophysical data processing and interpretation.

The DMA approach is utilized for an automated multi-criteria recognition of artificial and natural anomalies in the observatory geomagnetic data in the HSS developed at the GC RAS. Concept of the local indicators is based on dividing the initial record into several categories using the anomalousness levels, for instance the background level, weakly anomalous, anomalous, strongly anomalous levels. The parameter of anomalousness  $MA$  which varies in the range of  $[-1, 1]$  is calculated using the method described in [Soloviev et al., Estimation of geomagnetic activity..., Annals of Geophysics, in press]. The scale of anomalousness is universal for the whole range of actual records. It includes 4 grades:

- $-1 \leq MA(t) < 0.4$  for background values;

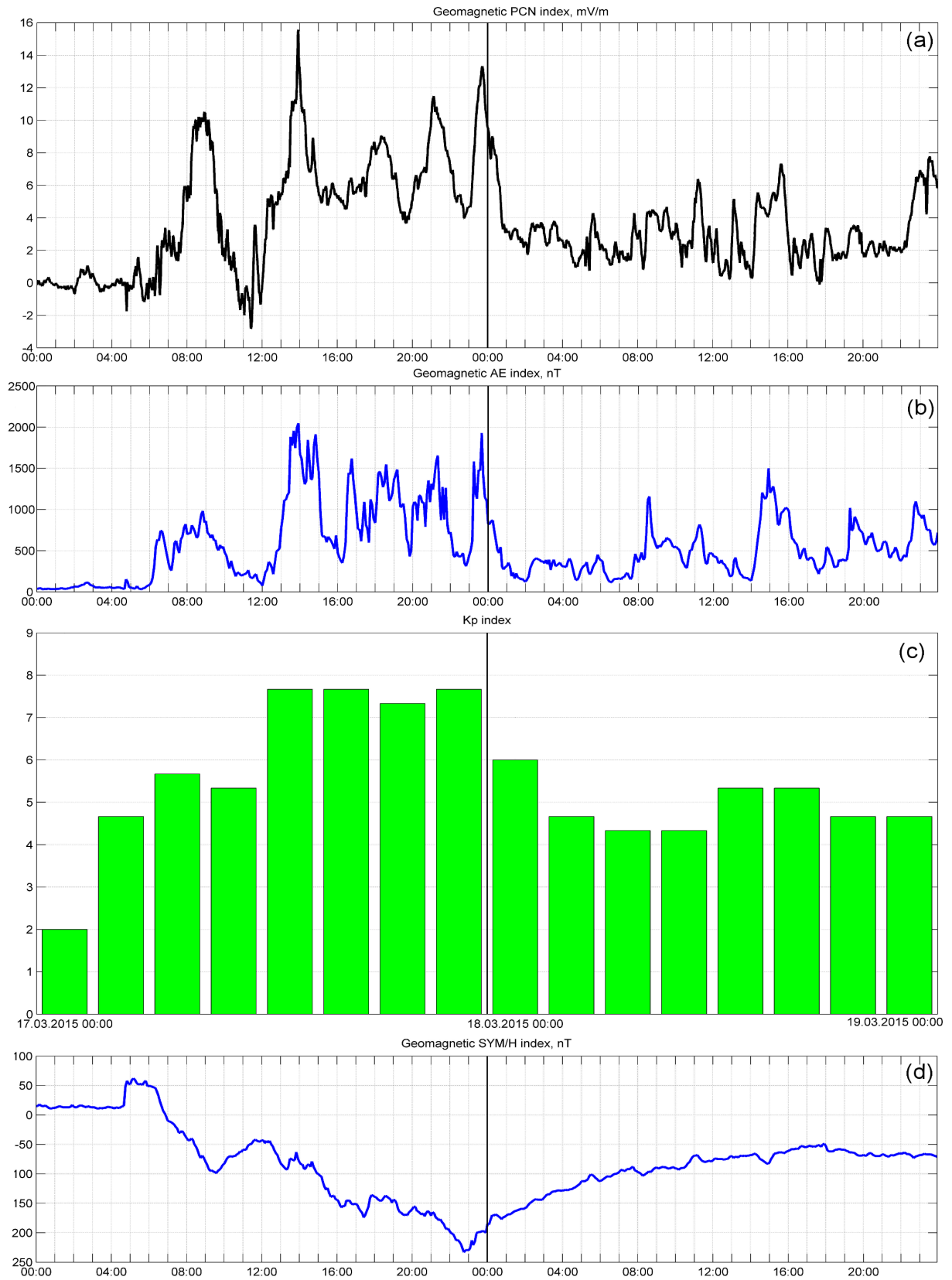


**Figure 2.** Geomagnetic indices for the St. Patrick's Day storm period: 1-min *PC* (a), *AE* (b), 3-hour *Kp* index (d), and *SYM/H* (c) indices.

- $0.4 \leq MA(t) < 0.55$  for weakly anomalous fragments of the time series;
- $0.55 \leq MA(t) \leq 0.7$  for anomalous fragments;
- $0.7 \leq MA(t) \leq 1$  for strongly anomalous fragments.

For the geomagnetic records the data analysis is performed for the 3-day period before a given time instant. This time period is considered as the optimal and representative to analyze the majority of geomagnetic disturbances. For a particular period, the local indicators could be derived for any observatory whose data is stored in the geomagnetic database. List of the local indicators of geomagnetic activity includes:

1. Recognition of natural anomalies using the measure of anomalousness ( $MA$ );
2. Estimation of geomagnetic disturbances by its maximum rate of change ( $dB/dt$ ,  $B$  is the magnetic induction vector) during 1 hour ( $E$ );
3. Estimation of geomagnetic disturbances by its and amplitude during 1 hour ( $A$ );
4. Operational  $K$  index calculation ( $K$ ).

To date, the geomagnetic data base included to the HSS collects and stores the data from 12 geomagnetic observatories located in the different regions of Russian Federation. The list of observatories along with its IAGA codes and geographic coordinates is given in Table 1. Most of the observatories are located at midlatitudes.

To illustrate how the local indicators describe the geomagnetic activity during the St. Patric's Day magnetic storm we apply the indicators (1)–(4) to the horizontal geomagnetic components measured at two observatories from Table 1: St. Petersburg (SPG) and Khabarovsk (KHB) located at  $60.542^\circ\text{N}$  and  $47.610^\circ\text{N}$ , respectively. The KHB is a typical midlatitude observatory, while the SPG is located closer to the auroral latitudes. Thus the data from KHB and SPG are representative for the different geomagnetic disturbance. In particular, the KHB magnetometer is likely more sensitive to the magnetic signal of the ring current, while the SPG magnetometer detects mostly the auroral electrojets.

Figure 3 depicts the actually measured geomagnetic  $X$  component and four local indicators, anomalousness  $MA$ , rate of disturbances  $dB/dt$ , amplitude of disturbances  $A$  and  $K$  index, calculated for SPG during the period of March 17–18. Concept of the local indicator  $MA$  is based on a dividing the initial record into several categories using a given levels of anomalousness. For instance in Figure 3a the background, marginally anomalous, mildly anomalous and strongly anomalous level is shown in blue, green, purple and red, respectively. The local indicator  $E$  (Figure 3b) for estimation of geomagnetic disturbances by its rate has a common physical meaning as the induced electric field ( $E \sim dB/dt$ ). This indicator is calculated on 1-hour or 3-hour basis. The indicator for estimation of geomagnetic disturbances by the amplitude  $A$  (Figure 3c) is calculated for the individual sporadic variation ranges at an individual

**Table 1.** Russian Magnetic Observatories. The INTERMAGNET Magnetic Observatories (IMOs) are Marked \*

Name	IAGA code	Geogr. Lat. (deg.)	Geogr. Long. (deg.)
Arti *	ARS	56.433	58.567
Borok *	BOX	58.068	38.233
Cape Schmidt	CPS	68.878	−179.370
Irkutsk *	IRT	52.165	104.460
Khabarovsk *	KHB	47.610	134.690
Klimovskaya	KLI	60.856	39.519
Kazan	KZN	55.910	48.790
Magadan *	MGD	60.051	150.728
Novosibirsk *	NVS	54.850	83.242
Paratunka *	PET	52.971	158.248
St. Petersburg *	SPG	60.542	29.716
Yakutsk *	YAK	61.960	129.660

magnetic observatory. In the HSS, this indicator is calculated on 1-hr, 3-hr and 24-hr basis. The operational local  $K$  index (Figure 3d) is considered as a real time general estimation of the geomagnetic disturbances in comparison with the corresponding quiet level. In the frame of HSS the quiet level is calculated for each day taking into account the previous 30 days and then the  $K$  index is computed.

Figure 4 depicts the same parameters as Figure 3 but for KHB.

### 3. Discussion

In order to determine the efficiency of the local indicators for the estimation of geomagnetic activity, let us compare them with the classical geomagnetic indices. The comparison between the results of geomagnetic activity analysis inferred from the parameter  $MA$  and the  $K$  index shows a good agreement in estimation of the storm time disturbances. In particular, just after the SSC the  $Kp$  index increases up to 5−, and the parameter  $MA$  increases up to 0.6–0.7, indicating that the geomagnetic conditions are considered potentially anomalous. During the storm main phase, when  $Kp = 7 + \dots 8$ − the parameter keep the value of 0.8–0.9 with the maximums corresponding to large natural peaks. In Figure 3 and Figure 4 all this period for  $MA$  is shown in red or purple indicating strongly disturbed conditions. On March 18, during the storm recovery phase the indicator oscillates between −0.5 and 0.5 with some insignificant weakly anomalous fragments which corresponds to the  $Kp$  values of 5+. Hence, the results of analysis using this indicator practically agree with the planetary  $Kp$  index evolution. For SPG (Figure 3), the results of estimation of geomagnetic disturbances by its rate and amplitude are in agreement with the  $AE$  index evolution. In particular, the periods of extreme  $AE$  index at 1300–1600, 1625–1950, 2000–2210 and 2300–0100 UT on March 17 are collocated with the extreme (strongly anomalous) periods of the rate

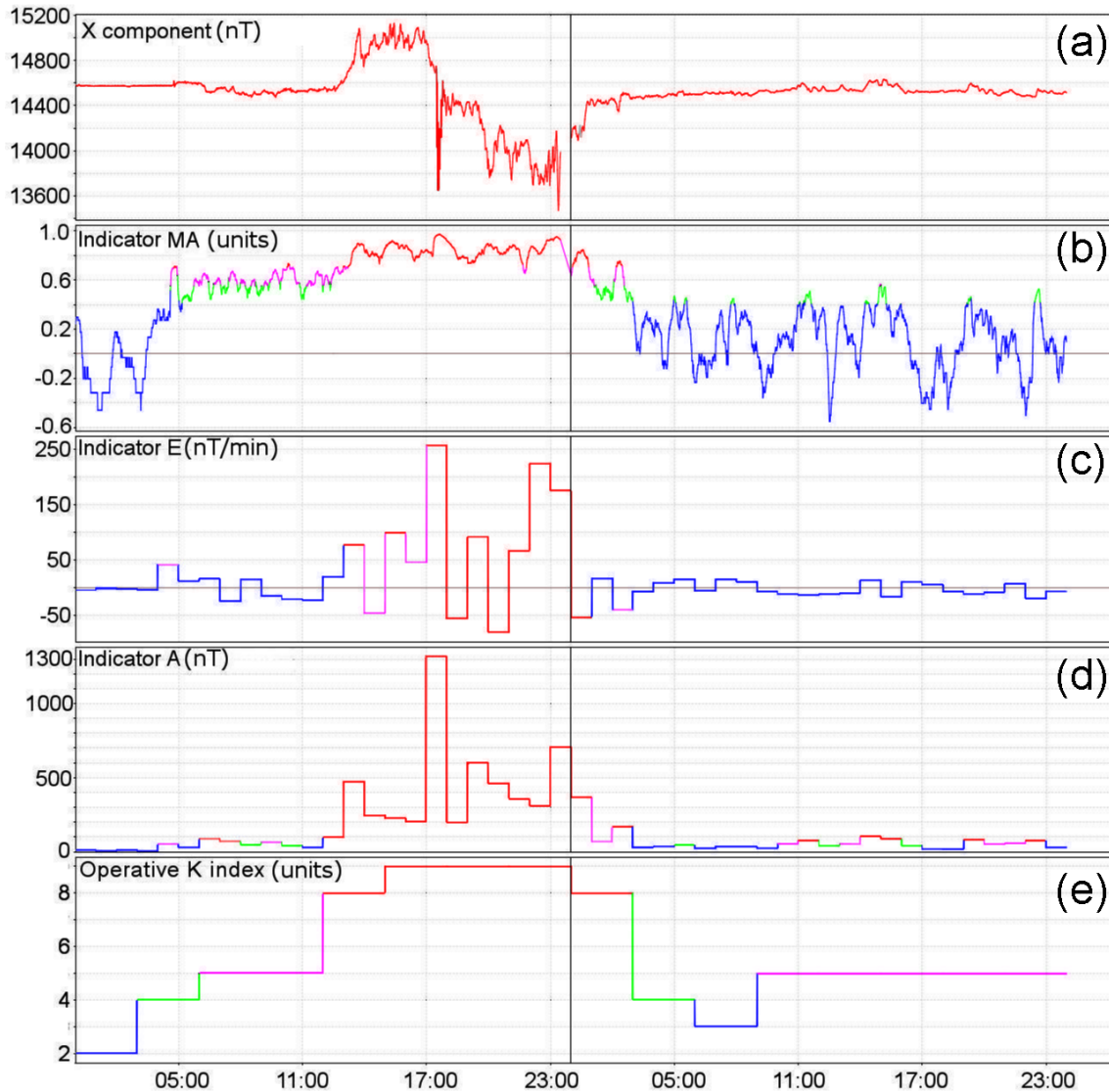


**Figure 3.** Data from the SPG observatory for the period of March 17–18, 2015: the actually observed geomagnetic  $X$  component (a), parameter of anomalousness  $MA$  (b), rate of disturbances  $E$  (c), amplitude disturbances  $A$  (d), and operational  $K$  index (e). the background, marginally anomalous, mildly anomalous and strongly anomalous level is shown in blue, green, purple and red, respectively.

and amplitude parameters. According to the indicator for estimation the disturbances by the rate of change, the strong level of anomalousness corresponds to the periods beginning from 1400, 1500 and 1700 UT. Large oscillations of the time derivatives after 1700 UT can be observed both in the SPG observatory  $X$  component and the  $AE$  index. Estimation of the amplitudes shows that the storm main phase period is considered strongly anomalous. Also one can see some agreement between this indicator and  $Kp$  data, though not so clear as in the previous case.

For KHB (Figure 4), the total range of variation is about 240 nT which is approximately 10 times less than the range for the SPG observatory. The KHB observatory is located in

the mid-latitude region and registers only the remote signal of the auroral electrojet. During the St. Patrick's Day storm several substorms occurred, however the  $H$  component from KHB does not follow the variation of the  $AE$  index. Instead, the KHB magnetometer records mainly the magnetic signal of the ring current. The shape of actually measured variation in  $H$  component is generally similar to the SYM/H index which represents the magnetic effect of the equatorial ring current. The results of the analysis using the local indicator  $MA$  show that the activity was enhanced during the storm main phase. However, the number and duration of strongly anomalous periods is smaller compared to the SPG observatory. The observed  $H$  component, its time derivative

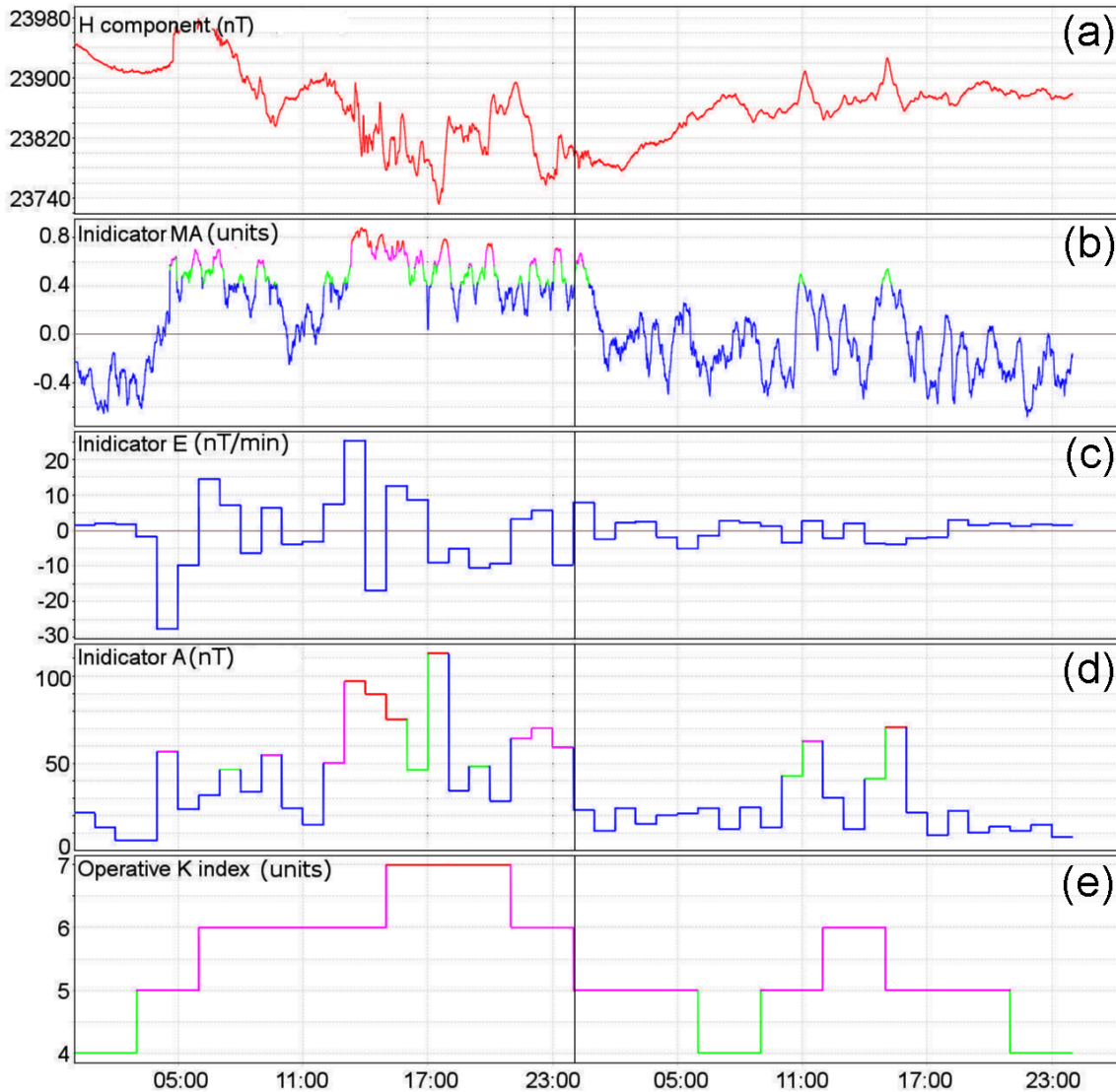


**Figure 4.** Data from the KHB observatory for the period of March 17–18, 2015: the actually observed geomagnetic  $H$  component (a), parameter of anomalousness  $MA$  (b), rate of disturbances  $E$  (c), amplitude disturbances  $A$  (d), and operational  $K$  index (e).

and its hourly averaged amplitude do not exhibit prolonged periods of large variations. This explains the absence of anomalous fragments in the indicator  $E$  (the corresponding periods are marked in blue) and the presence of only few short and isolated anomalous fragments for the indicator  $A$ . All the anomalous and strongly anomalous fragments match the peaks on  $H$ .

Comparing the second and fourth panels in Figure 3 and Figure 4, one can see that under the storm time conditions the operational local  $K$  indices usually vary in accordance with the parameter of anomalousness calculated for each observatory. While the planetary index  $Kp$  differs in detail from the local indicators, all of them are significantly enhanced during the same period of time.

#### 4. Conclusions

Comparison of the results of geomagnetic activity monitoring using the local indicators with the traditional geomagnetic indices for geomagnetic activity analysis during St. Patrick's Day magnetic storm demonstrated that the classification of magnetic activity using the mentioned indicators is in agreement with the classical methods. The main conclusions are the following:

1. The local indicators, applied to recognition of geomagnetic disturbances in the observatory data seem an effective tool for geomagnetic activity analysis. The approaches allow determining the gradations of

anomalousness in geomagnetic records. The geomagnetic activity estimations using the local indicators reveal the characteristic features of geomagnetic disturbances typical for the observatory latitudinal location. These results show a good agreement with the conventional geomagnetic disturbance distribution and its evolution during a magnetic storm.

2. The effectiveness of the parameter of anomalousness is similar to the classical geomagnetic  $K$  index. This parameter could be considered as an advanced approach to geomagnetic monitoring, due to its realtime operation and the same temporal resolution as the initial cadence of measurements.
3. The local indicators for estimation of the rate of geomagnetic disturbances and its amplitude provide an overall dynamic image of the disturbed period. In the particular case of magnetic storm, these indicators generally match the  $AE$  index variations. Further analysis will be performed in the future, including comparison of different data sets for different auroral and subauroral magnetic observatories.

**Acknowledgments.** The research has been carried out in the framework of the Federal target program of the Ministry of Education and Science of the Russian Federation, agreement No. 14.607.21.0058, project unique identifier RFMEFI60714X0058, and is a part of research aimed at the creation of the experimental prototype of the HSS for monitoring and detection of extreme geomagnetic phenomena using ground-based and satellite data.

## References

- Agayan, S. M., Sh. R. Bogoutdinov, M. N. Dobrovolsky, et al. (2014), Weighted gravitational time series smoothing, *Russ. J. Earth. Sci.*, *14*, ES3002, doi:10.2205/2014ES000543
- Agayan, S., Sh. Bogoutdinov, A. Soloviev, R. Sidorov (2016), The Study of Time Series Using the DMA Methods and Geophysical Applications, *Data Science Journal*, *15*, 1–21, doi:10.5334/dsj-2016-016
- Agayan, S. M., A. D. Gvishiani, S. R. Bogoutdinov, A. I. Kagan (2010), Smoothing time series using methods of discrete mathematical analysis, *Russ. J. Earth Sci.*, *11*, RE40001, doi:10.2205/2009ES000436
- Bogoutdinov, Sh. R., et al. (2010), Recognition of Disturbances with Specified Morphology in Time Series. Part 1: Spikes on Magnetograms of the Worldwide INTERMAGNET Network, *Izvestiya, Physics of the Solid Earth*, *46*, No. 11, 1004–1016.
- Davis, T. N., M. Sugiura (1966), Auroral electrojet activity index  $AE$  and its universal time variations, *J. Geophys. Res.*, *71*, 785–801.
- Dungey, J. W. (1961), Interplanetary magnetic field and the auroral zones, *Phys. Rev. Lett.*, *6*, 47–48, doi:10.1103/physrevlett.6.47
- Gvishiani, A. D., S. M. Agayan, S. R. Bogoutdinov, A. I. Kagan (2011), Gravitazionnoe sglazhivaniye vremennyh ryadov (Gravitational smoothing of time series), *Tr. IMM UrO RAN*, *17*, No. 2, 62–70. (in Russian)
- Gvishiani, A., R. Lukianova, A. Soloviev, A. Khokhlov (2014), Survey of Geomagnetic Observations Made in the Northern Sector of Russia and New Methods for Analysing Them, *Surveys in Geophysics*, *35*, No. 5, 1123–1154, doi:10.1007/s10712-014-9297-8
- Gvishiani, A., et al. (2016a), New hardware and software complex for monitoring and analysis of the Earth's magnetic environment. Kedrov E. (ed.) Book of Abstracts of the International Conference “Data Intensive System Analysis for Geohazard Studies”, *Geoinf. Res. Papers Ser.*, *4*, BS4002, doi:10.2205/2016BS08Sochi
- Gvishiani, A., A. Soloviev, R. Krasnoperov, R. Lukianova (2016b), Automated hardware and software system for monitoring the Earth's magnetic environment, *Data Science Journal*, *15*, No. 18, 1–24. doi:doi: 10.5334/dsj-2016-018
- Iyemori, T., T. Araki, T. Kamei, M. Takeda (1992), *Mid-latitude geomagnetic indices ASY and SYM (Provisional) No. 1, 1989*, Data Anal. Center for Geomagn. and Space Magn., Kyoto Univ., Kyoto, Japan.
- Menvielle, M., A. Berthelier (1991), The K-derived planetary indices: description and availability, *Rev. Geophys.*, *29*, No. 3, 415–432.
- Rasson, J. L. (2001), The status of world-wide network of magnetic observatories, their location and instrumentation, *Contributions to Geophysics and Geodesy*, *31*, 427–453.
- Richardson, I. G., H. V. Cane (2012), Solar wind drivers of geomagnetic storms during more than four solar cycles, *J. Space Weather Space Clim.*, *2*, 9, doi:10.1051/swsc/2012001
- Soloviev, A. A., et al. (2012a), Recognition of Disturbances with Specified Morphology in Time Series: Part 2. Spikes on 1-s Magnetograms, *Izvestiya, Physics of the Solid Earth*, *48*, No. 5, 395–409.
- Soloviev, A. A., et al. (2009), Detection of hardware failures at INTERMAGNET observatories: application of artificial intelligence techniques to geomagnetic records study, *Russ. J. Earth Sci.*, *11*, ES2006, doi:10.2205/2009ES000387
- Soloviev, A., S. Bogoutdinov, A. Gvishiani, R. Kulchinskiy, J. Zlotnicki (2013), Mathematical Tools for Geomagnetic Data Monitoring and the INTERMAGNET Russian Segment, *Data Sci. J.*, *12*, WDS114–WDS119, doi:10.2481/dsj.WDS-019
- Soloviev, A., et al. (2012b), Automated recognition of spikes in 1 Hz data recorded at the Easter Island magnetic observatory, *Earth Planets Space*, *64*, No. 9, 743–752, doi:10.5047/eps.2012.03.004
- Troshichev, O. A., et al. (1988), Magnetic activity in the polar cap-A new index, *Planet. Space Sci.*, *36*, 1095.
- Zelinskiy, N. R., N. G. Kleimenova, O. V. Kozyreva, et al. (2014), Algorithm for recognizing Pc3 geomagnetic pulsations in 1-s data from INTERMAGNET equatorial observatories, *Izvestiya, Physics of the Solid Earth*, *50*, No. 2, 240–248.
- A. D. Gvishiani, R. Yu. Lukianova, R. V. Sidorov, A. A. Soloviev, Geophysical Center RAS, Molodezhnaya St. 3, 119296, Moscow, Russia. (r.sidorov@gcras.ru)